Kinetics of cyclically-induced mechanical twinning in γ-TiAl unveiled by a combination of acoustic emission, neutron diffraction and electron microscopy

*A. Vinogradov[1], M. Heczko[*2,3], V. Mazánová[*,3], M. Linderov[4] and T. Kruml[2,3]*

[1] Department of Mechanical and Industrial Engineering, Norwegian University of Science and Technology - NTNU, Trondheim, N-7491, Norway
[2] CEITEC, Institute of Physics of Materials, Brno, Czech Republic
[3] Institute of Physics of Materials, The Czech Academy of Sciences, Brno, Czech Republic
[4] Institute of Advanced Technologies, Togliatti State University, Togliatti 445020, Russia

Abstract

The cyclic response and the microstructure evolution of the near γ-TiAl alloy are investigated by a blend of contemporary experimental techniques centred around in-situ acoustic emission (AE) measurements reflecting the cyclically-induced structural changes in the real-time scale. TEM and SEM – ECCI/EBSD examinations provided an adequate qualitative description of microstructural features associated with populations of dislocations and mechanical twins evolving concurrently in the course of cyclic deformation. Since the TEM offers only local and post-mortem information, the in-situ neutron diffraction technique scanning a large part of the gauge length was employed to characterise the lattice strain distributions with cycling. The volume fraction of twins as a function of loading cycles was obtained after loading or unloading half-cycles. The processes controlling the cyclic strain hardening during each deformation cycle were assessed by (i) the statistical analysis of the shape of the hysteresis loop aiming at the characterisation of distribution internal stress barriers for deformation mechanisms involved and (ii) the spectral and statistical analysis of AE data providing information on the kinetics of these mechanisms. Each of the used experimental methods brings its own set of advantages and limitations in terms of characterisation and interpretation. Their unique combination ensures a host of benefits that promote a comprehensive understanding of primary deformation mechanisms - deformation twinning, dislocation slip and detwinning. It is shown that the cyclic mechanical behaviour of the TiAl alloy can be comprehensively explained by the interplay between these mechanisms co-operating during each loading cycle. This interplay governs the behaviour of underlying mechanisms in the early stages of the fatigue damage evolution and likely determines the overall fatigue response of near γ-TiAl alloy at room temperature.

Keywords: TiAl alloy; cyclic deformation; dislocation slip; twinning; microscopy; neutron diffraction; acoustic emission

[*] *Present address: The Ohio State University, Department of Materials Science and Engineering, Center for Electron Microscopy and Analysis (CEMAS), 1305 Kinnear Rd, Suite 100, Columbus, OH 43212, USA.*

1. Introduction

The combination of low density, high strength and excellent corrosion resistance of gamma-based titanium aluminides at high temperatures [1, 2] has made this class of materials attractive to further development for high-temperature applications with extensively improved cost-efficiency. However, the lower than expected fatigue and fracture properties at both room and high temperatures and the overall poor ductility and machinability still leave a lot to desire for [3-5]. Thus, the development of the TiAl alloys is far from being completed. The motivation for the burgeoning research in this field is driven by the successful incorporation of a few TiAl variants into real structural applications working at elevated temperatures up to 750°C. One of such materials is the "Alloy 48-2-2", in particular, Ti-48Al-2Nb-2Cr (at.%), which has been already tested in low-pressure parts of aircraft engines or turbochargers in the automotive industry [6].

TiAl alloys can be fabricated through thermo-mechanical routes to different microstructures including equiaxed (near γ), duplex and lamellar. It is frequently claimed that the lamellar microstructure, where fine layers of γ and α_2 phases alternate, shows the best properties as, e.g. the enhanced resistance to crack propagation [7]. However, this is true only when the lamellae are suitably oriented with respect to the crack propagation path [8]. If the lamellae are parallel to the stress axis, they indeed act as natural barriers for gliding dislocations as well as for the growth of small fatigue cracks. On the other hand, the fatigue cracks propagate very rapidly along the interphase boundaries in the grains where the lamellae are perpendicular to the stress axis [9]. Since the fabrication of TiAl alloys by casting produces polycrystals typically with very coarse grains of more than 1 mm in size, the statistical distribution of lamellae orientation in grains within the gauge length of the specimens may vary for different specimens, contributing to the significant scatter of fatigue lives, which is usually reported for the TiAl alloys [3, 10]. Therefore, it is essential to gain a better understanding of the deformation behaviour of TiAl alloys produced in the microstructural states other than the fully lamellar ones. Several studies suggested that the tensile elongation to fracture could be higher for the alloy with the near γ microstructure than that for the lamellar alloy [11]. In following up this strategy, the present work deals with the material having the chemical composition close to the "Alloy 48-2-2", yet with the near γ microstructure. To gain a better understanding of macroscopic mechanical properties, the effort is put on revealing the deformation mechanisms governing the response of the alloy to external loads. It has been well-understood that, besides dislocation glide and climb, the mechanical twinning plays an essential role in the plastic flow of the near-γ TiAl alloy with a given specific composition and microstructure [12]. While twinning is often considered insignificant for plastic flow in many ductile materials, it is thought to be beneficial for the γ-phase ductility because of insufficient slip systems: there are only four slip systems where slip of ordinary dislocations can be activated. To fulfil the von Mises criterion of plasticity requiring five independent deformation systems to accommodate an arbitrary deformation [13], either slip of superdislocations or twinning must be activated (see [14, 15] for the survey of deformation mechanisms involved in plastic flow of γ-TiAl). The crystallographic aspects of deformation twinning in the near γ-TiAl alloys with the ordered $L1_0$ structure have been discussed by Skrotzki in great details [16].

The significance of mechanical twinning in monotonic tensile or compressive loading of γ-TiAl has been underlined by using the acoustic emission (AE) measurements. This technique has long been proven efficient for twinning detection since the rapid appearance of twins is accompanied by distinct acoustic effects [17]. Kauffmann [18] et al. and Marketz et al. [19] have performed the analysis of the AE activity in the fine-grain texture-free γ–TiAl based alloys produced by powder metallurgy routes. The average size of γ-grains was of 7 μm. The samples were monotonically tested in compression with different strain rates. The AE was primarily associated with deformation twinning. The sharp AE peak was observed systematically

around the yield point, similarly to that in the vast majority of structural metals and alloys [20]. The reduction in the AE activity beyond the 0.5% total compressive strain was attributed to the prevalence of the dislocation slip with increasing strain. Besides, it was reasonably suggested that the newly formed mechanical twins have a shorter length since the already existing twins act as obstacles for the lengthwise twin propagation. As the AE amplitude is linearly related to the twin length [21], the shorter the twin, the smaller the AE signal. Similar findings were reported by Viswanathan et al. [11] for the Ti-48Al alloy tested in tension. Twinning was also evidently observed in the deformed microstructure and correlated with AE. Besides, the microcracks were found in the fractured specimens, and these were also supposed to be the sources of the measured total AE. The microcracks as the sources of AE in the duplex or fully lamellar TiAl alloys have been in the focus of dedicated investigations by Botten et al. [22, 23] and Hu et al. [24].

Real components in service are usually subjected to variable or periodically changing loads. Therefore, an understanding of the cyclic plastic response of the alloy and the associated interplay between the two major deformation modes - dislocation slip and twinning - is of paramount importance not only for the assessment of the fatigue life but also for the potential thermomechanical processing treatments involving deformation steps with strain reversal.

Conflicting results have been reported in this regard. In general, the increasing content of solute atoms tends to suppress twinning. Therefore, twinning as one of two primary deformation modes in α-Ti is supposed to be significant only in pure Ti [25]. Several reports [16, 26-28] indicate that the deformation twinning does not play an essential role in the increase of the cyclic strength of the γ-phase since the coherent twin boundaries represent only minor obstacles to dislocation motion and, therefore, the dislocation slip serves as the primary mechanism of cyclic hardening. As opposes to this, Appel et al. [1] followed later by Hénaff and Gloanec [10] supported the idea that cyclic hardening is related to the prevailing mechanical twinning, which delays the formation of tangled dislocation structures. In the present work, this controversial topic is revisited from a perspective that seeks to compare and rationalise the results obtained from a blend of microscopic and in-situ deformation techniques including the neutron diffraction, transmission electron microscopy (TEM) [12], electron channelling contrast imaging (ECCI) in scanning electron microscopy (SEM) and the acoustic emission technique complemented by the statistical analysis of the shape of the hysteresis loop. This characterisation strategy brings new insights into the material response during cyclic plastic loading as will be discussed in detail below.

2. Experimental details

2.1. Material

The investigated material was titanium-aluminide alloy Ti-48Al-2Nb-2Cr-0.82B (at. %) with the near gamma microstructure, received in the form of cast bars of 57 mm diameter and 200 mm length from GfE Metalle und Materialien GmbH (Nürnberg, Germany). The average grain size was about 46 µm. However, the grain dimensions varied broadly, and the grains exceeding 200 µm in diameter were also observed in the microstructure. The initial microstructure was characterised in detail, as reported in the following sections.

2.2. Electron microscopy

The microstructural characterisation was performed on the oriented TEM foils. Thin plates were cut from the gauge length of the bulk specimens by the electric-discharge machine at the angle of 45°, perpendicular and parallel to the loading axis. The samples were mechanically ground to produce thin plates with a thickness of 0.1 mm, from which the discs with a diameter of 3 mm were punched out. These were marked to indicate the loading direction. The discs were then electrolytically polished. The electrolyte was composed of 85% of ethylalcohol, 8% of perchloric acid and 7% of butylalcohol. The polishing was conducted at 40–50 V, 200 mA and temperature of −40 °C to −55 °C. The initial state of the material was examined using the TEM foils prepared from the as-received ingot.

The microstructure of the studied material was analysed using the dual-beam SEM Tescan LYRA 3 XMU FEG equipped with the electron backscatter diffraction (EBSD) detector by Oxford Instruments operated with the Oxford Aztec software. The electropolished TEM foils were placed into the special holder enabling characterisation in the SEM chamber. The accelerating voltage of 20 kV and the spot size of 60 nm were used to collect the high-resolution EBSD maps. All investigated material states were characterised in the backscattered electrons (BSE) imaging mode. The accelerating voltage of 10 kV and the working distance of 6 mm were used to recognise the individual grains and deformation twins using the ECCI technique.

Scanning transmission electron microscopy (STEM) was employed for the high-resolution characterisation of the microstructure. The foils were tilted to perform high-angle annular dark-field (HAADF) zone axis imaging using an image-corrected and monochromated Thermo Fisher Scientific/FEI Titan-Themis 60-300 kV S/TEM also equipped with the Super-X energy-dispersive X-ray spectroscopy (EDS) detector. The atomic resolution STEM images were corrected for possible drift and scanning beam distortions using the drift corrected frame integration (DCFI) function built-in in the Velox software.

2.3. Cyclic tests

The cyclic mechanical tests were performed in the fully reversed tension-compression axial mode under total strain-control using a clip-on extensometer. All tests were carried out in air at ambient temperature. Three different testing rigs were employed depending on the purpose.

The in-situ deformation experiments using the neutron diffraction source were performed using the diffractometer POLDI located at the Swiss Neutron Spallation Source at the Paul Scherrer Institute. The testing rig with a 30kN maximal force was used to strain the cylindrical specimens with 6 mm gauge part diameter as described in [12]. These tests were performed in the interrupted mode to enable diffraction measurements along the strain path.

To perform the statistical analysis of the shape of the hysteresis loops, the stress-strain data need to be obtained with higher resolution. This has been done in a series of conventional low-cycle fatigue tests employing the servohydraulic testing machine MTS 810 equipped with the Teststar IIs digital control unit. 2000 stress-strain readings were collected per cycle. The total cyclic strain rate was kept constant at 2×10^{-3} s^{-1}. The flat dog-bone specimens with the square cross-section of 3×3 mm^2 and the gauge length of 8 mm were used. All specimens were carefully mechanically polished to a mirror-like finish prior to testing.

The acoustic emission measurements were carried out under the same testing conditions using a rigid screw-driven mechanical testing machine Kammrath&Weiss with up to 10 kN load-bearing capacity. The constant crosshead velocity of 5 μm/s was maintained for this series of tests.

The total strain amplitudes of ε_a=0.2% and 0.4% were applied in all three testing campaigns. As all the specimens undergo the same type of loading, it can be reasonably assumed that the results obtained by different characterisation techniques are applicable to all tests.

2.4. Neutron diffraction

The time-of-flight neutron diffractometer with a wavelength range of 0.1–5 nm was used. The data analysis provided access to the evolution of the lattice strains on γ-phase planes {110} [29], {112} and {123} during cycling. Additional details can be found in [12].

2.5. Acoustic emission

In the AE tests, the piezoelectric sensor PICO (MISTRAS, USA) with a frequency band of 200-1000 kHz was attached to the undeformed shoulder part of the specimen in close proximity to the gauge part. Vacuum oil was used as a coupling medium to ensure efficient transfer of elastic waves from the surface to the transducer. The AE signals were amplified by 60 dB in the frequency band from 50 to 1200 kHz by the low-noise pre-amplifier 2/4/6 and recorded by the 16-bit PCI-2 data acquisition board (MISTRAS, USA) operated in the "thresholdless" mode at the sampling rate of 2 Msamples/s.

The continuously streamed data were sectioned into *N* consecutive individual realisations of 4k samples without overlapping. A Fourier power spectral density (PSD) function $G(f)$ was calculated from these data using a Welch method. The average per realisation *AE power* P_{AE} was calculated from the corresponding PSD as $P_{AE}=\int_{f_{\min}}^{f_{\max}} G(f)\,df$. The *median AE frequency* f_m was introduced through the implicit equation $\int_0^{f_m} G(f)\,df=\int_{f_m}^{\infty} G(f)\,df$. Both P_{AE} and f_m were obtained from $G(f)$ after subtraction of the PSD of the laboratory noise pre-recorded before the start of loading during each test. The sectioned AE data set was statistically analysed employing the adaptive sequential *k*-means clustering (ASK) technique proposed in [30] to discriminate between different AE sources. Different deformation and fracture mechanisms such as dislocation slip, twinning and microcracks are supposed to generate different waveforms [31], resulting, consequently, in different PSDs (see [32-34] for examples and implementations of the ASK method). The normalised PSD functions $\tilde{G}(f)=G(f)/P_{AE}$ characterising each AE realisation were used as input for the ASK algorithm, which compared the pairwise difference between all $\tilde{G}_i(f)$ for $i\in[1,N]$ using a symmetrical version of the Kullback-Leibler divergence as a statistical measure of similarity between data sets. Mathematical details of this classifier are discussed in [30]. The two most important features of the ASK method to be mentioned are: (i) the number of clusters to be derived from a dataset is 'data-driven' and is not specified a priori, and (ii) the process is non-iterative, i.e. the AE signals are associated with a certain cluster sequentially as they arrive one after another.

3. Results

3.1 Initial microstructure

The initial state of the studied near γ-TiAl alloy was characterised using electron microscopy. The SEM-EBSD scan reveals the typical microstructure and grain distribution in Fig. 1a. The detailed fragment, Fig. 1b, shows equiaxed grains which can contain annealing twins and secondary phases. Collecting and summing up the data from several EBSD scans, the grain size distribution was plotted as the histogram fitted by the log-

normal distribution function in Fig. 1c. The maximum of the distribution corresponding to the most probable grain size is of 25 µm, the mean value is of 46 µm and the standard deviation is of 28 µm.

The secondary phases were unveiled and assessed by TEM. The structural parameters of expected phases were extracted from the detailed study by Beran et al. [35]. They were then used as the input variables for the EBSD software. The raw high-resolution EBSD phase map was obtained and correlated with the band contrast image to precisely identify the locations of different phases. The phase map was then manually coloured to highlight and discriminate between different phases detected in the scanned area (Fig. 2a). The structure and chemical composition of phases were identified by the selected area electron diffraction (SAED), STEM-EDS (not shown here) and high-resolution HAADF-STEM. In addition to the tetragonal γ-TiAl matrix, a small amount of the hexagonal α_2-Ti_3Al phase was found (Fig. 2b). This phase was observed as thin elongated plate-like needles, mostly oriented along {111}γ planes and maintaining the Blackburn orientation relationship with the γ-TiAl matrix: $\{111\}_\gamma \parallel \{0001\}_{\alpha 2}$ and $<1\bar{1}0]_\gamma \parallel <11\bar{2}0>_{\alpha 2}$ [†][36], as shown in Fig. 2c. The Cr-rich Ti_2AlCr particles were found in sparse locations, predominantly at the triple junctions or at the high-angle grain boundaries. This ordered Cr-rich phase with the cubic CsCl crystal lattice type has been reported in near γ-TiAl alloys with Cr additions larger or equal to 2 at.% [37]. It is important to note that the overall volume fraction of the secondary phases was very low, i.e. below 3%, as had been measured by the powder neutron diffraction method [12].

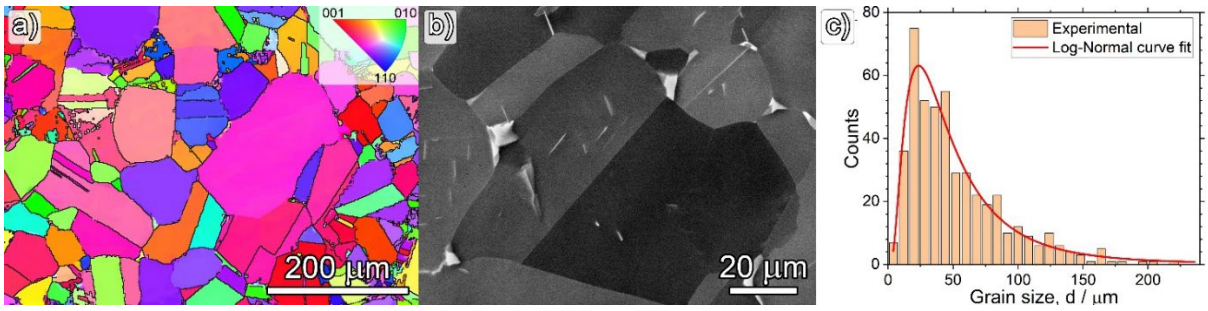

Figure 1: *(a) SEM-EBSD scan revealing the typical microstructure of the studied polycrystalline near γ-TiAl alloy in the initial state. (b) Equiaxed gamma grains* visualised in the *SEM-BSE mode can contain annealing twins and secondary phases. While thin elongated plate-like α_2-Ti_3Al phase can be found inside some grains, Cr-rich Ti_2AlCr phase is observed mostly at the triple junctions. (c) Grain size log-normal distribution determined from several EBSD scans.*

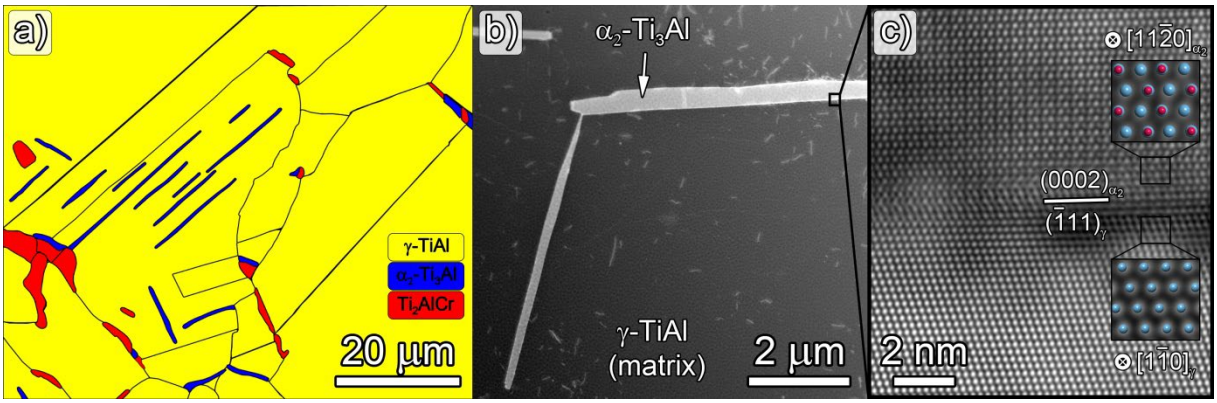

Figure 2: *(a) Post-processed coloured high-resolution SEM-EBSD phase map shows the typical distribution of α_2-Ti_3Al and Cr-rich Ti_2AlCr phases in the studied alloy. (b) HAADF-STEM image of thin elongated plate-like α_2-Ti_3Al phase in γ-TiAl matrix. (c) FFT (fast Fourier transform) filtered HAADF-STEM image of the α_2/γ interface observed along* $[1\bar{1}0]_\gamma // [11\bar{2}0]_{\alpha 2}$ *zone axes. Both phases maintain Blackburn orientation relationship. Ti and Al atoms are coloured in blue and red, respectively.*

[†] Mixed 〈hkl] notations are used to indicate the tetragonal lattice of the $L1_0$ phase.

3.2. Microstructure after cyclic loading

In the initial state of the alloy, no deformation twins are present in most of the grains (see the representative picture in Fig. 1b). To follow the production of the cyclically-induced deformation twins, SEM-ECCI was used to characterise the deformation microstructures. Examinations were performed in the specimens loaded with the total strain amplitudes of 0.2% (until fracture at 312 cycles) and ε_a=0.4% (after 2.5 cycles and until fracture at 32 cycles). Figure 3 unveils the contribution of twinning to the cyclic plastic deformation in individual γ-grains with a suitable crystallographic orientation enabling the channelling contrast on dislocations and deformation twins.

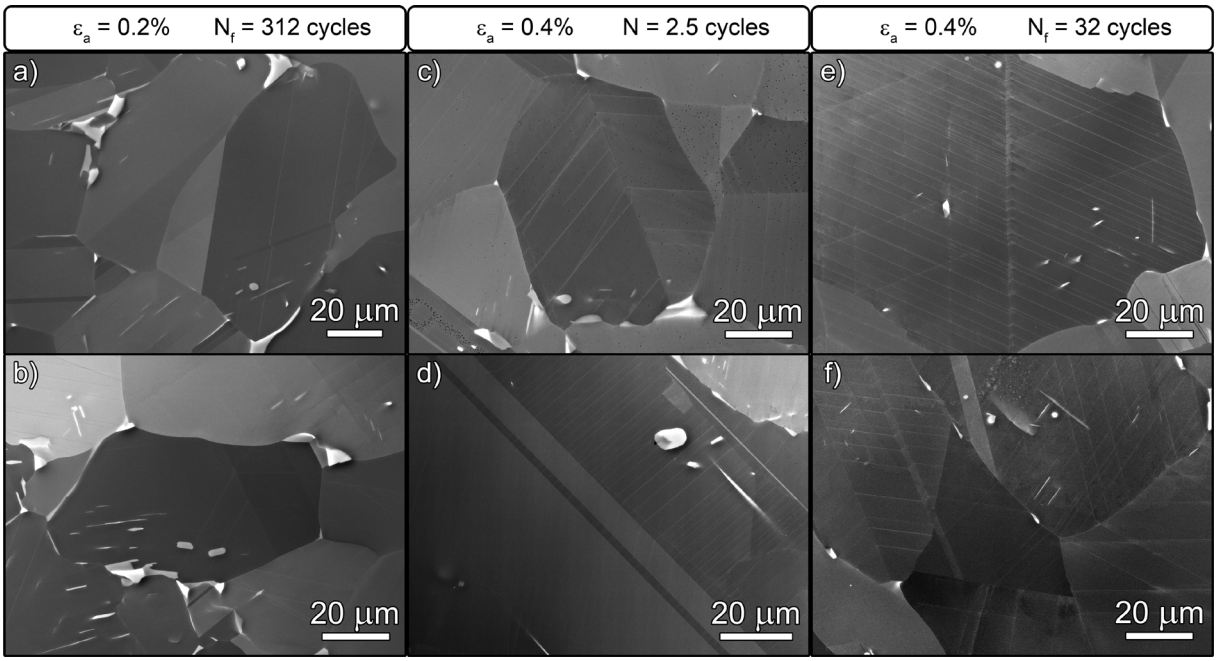

Figure 3: *SEM-ECCI analysis of the deformation twins populations in different states of the alloy. (a), (b) - the total strain amplitude ε_a =0.2%, loaded to fracture at 312 cycles. (c), (d) - the total strain amplitude ε_a =0.4%, loaded to 2.5 cycles. (e), (f) - the total strain amplitude ε_a =0.4%, loaded to fracture at 32 cycles.*

Even a qualitative juxtaposition of the initial and deformed microstructures reveals a notable increase in the density of mechanical twins with the increasing strain amplitude. While only a few twin lamellae are observed in the specimen tested at ε_a =0.2% (see Figs. 3a and b), the specimen cycled at 0.4% strain exhibits a much higher deformation twin density already after 2.5 cycles (see Figs. 3c and d). The overall fraction of deformation twins tends to rise further gradually with cycling as is witnessed by the visibly increased twin density after fracturing at 32 cycles (Figs. 3e and f). However, the twin fraction increment in the cycling interval from "the initial state" to "2.5 cycles" is observably more significant than in that from "2.5 cycles" to "fracture". For the cyclic loading at ε_a =0.4%, most of the twin activity is observed during the first 3-5 cycles. As will be discussed in what follows, these findings are in excellent agreement with the results of the independent acoustic emission analysis as well as with the outcomes of the in-situ neutron diffraction experiments [12].

Deformation twins were further analysed, and their thickness was determined to vary between 15 and 35 nm, depending on grain size and orientation. The low angle annular dark field (LAADF) STEM diffraction contrast image [38] in Fig. 4a reveals the typical substructure formed in response to the cyclic

loading. The observed microstructure was tilted so that the deformation twins of interest were oriented "edge-on", i.e. viewed along the $[\bar{1}10]_\gamma$ zone axis (see Fig. 4b). The obtained raw HAADF-STEM images were subjected to several processing steps and numerical analysis in order to enhance and emphasise the observed features by plotting the Centre of Symmetry (COS) maps. The purpose of the analysis was to locate and identify the degree of centro-symmetry for each atomic column. By measuring the deviation from the FCC atomic arrangement, in this case along the $\langle\bar{1}10\rangle$ zone axis, the precise locations of $(11\bar{1})_\gamma$ twinning planes and then the thickness of the deformation twins could be identified, c.f. Fig. 4c. All stages of the processing sequence were performed using MATLAB® with the Image Processing Toolbox [39, 40].

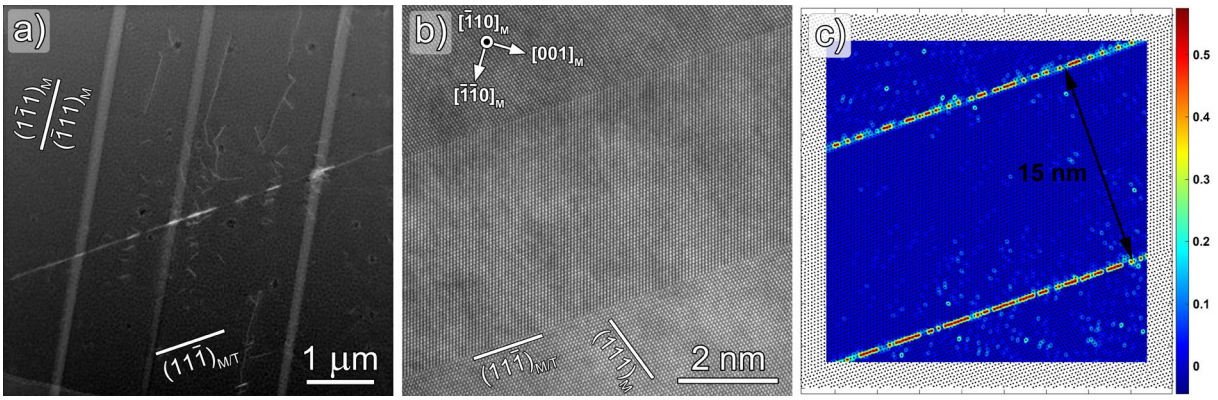

Figure 4: *Microstructure after cyclic loading with ε_a = 0.4% for 32 cycles until fracture. (a) LAADF-STEM diffraction contrast image showing two sets of deformation twins. (b) High-resolution HAADF-STEM image showing the characteristic deformation twin in the γ-TiAl matrix. The structure in (a, b) is viewed along the $[\bar{1}10]_\gamma$ zone axis. (c) The COS map highlighting the $(11\bar{1})_\gamma$ twinning planes, thus, enabling precise determination of the twin thickness.*

The evolution of the dislocation microstructure and the dislocation arrangement after cyclic straining under the same conditions has been investigated by TEM in great detail in the earlier work by Beran et al. [12]. It has been particularly shown that depending on the grain orientation, two types of grains with remarkably different microstructures are distinguished in the microstructure, c.f. also [41]. One group of grains contains a high density of deformation twins and low/medium density of dislocations in the form of either individually distinguishable dislocations or pile-ups. The other group of grains is featured by the low density of twins and the high density of tangled dislocations. Thus, the microscopy data underlines the significance of the interplay between both primary deformation modes – dislocation slip and twinning – which will be further unfolded in more detail by the AE analysis below.

3.3 Cyclic behaviour and statistical analysis of the hysteresis loops

Figure 5 shows the first cyclic hysteresis loops obtained in the alloy tested at two different strain amplitudes. It was experimentally verified that changing the direction of the first loading, i.e. starting the test in either tension or in compression, does not alter either the cyclic behaviour or the AE response. This observation concurs with the results reported by Gloanec et al. [42] for the effect of the initial loading direction on the cyclic stress-stress response in near-γ TiAl tested at the same ε_a. The shape of the hysteresis loop appears to be symmetrical in ascending and descending directions. The hysteresis loops do not exhibit any pronounced concavity or the plateau-like behaviour typical of hcp metals or TWIP steels, where the strain hardening behaviour is mediated by profuse twinning. This observation is in good agreement with results by Satoh et al.

[43] and Serrano et al. [44] who investigated the cyclic behaviour of the equiaxed near-γ TiAl intermetallics. Nevertheless, as will be shown below with aid from AE measurements, the mechanical twinning plays an essential role in the overall mechanical response of near γ-TiAl alloys.

The analysis of the cyclic response is based on the generalised statistical theory of the hysteresis loop proposed by Polák et al. [45, 46]. It is footed on the following assumptions: i) in agreement with the original Masing hypothesis [47], the whole volume of the specimen consists of many individual microscopic volumes arranged in parallel. When the external strain is applied, each microvolume yields depending on its critical shear stress, which consists of two components - the internal critical tensile (or compressive) stress, and saturated effective stress. The internal critical stress is the stress at which the microvolume starts yielding without hardening, provided the strain rate is infinitesimally low; ii) the individual elementary volumes are small enough to consider the internal stress to be constant in each of them; iii) the microstructure does not change considerably within one cycle, i.e. the internal stress does not change either; iv) the internal stress can be different in microscopic volumes, but the effective stress is the same in the entire specimen, v) the microscopic volume starts to yield plastically when the applied stress exceeds the sum of the internal and effective stress components.

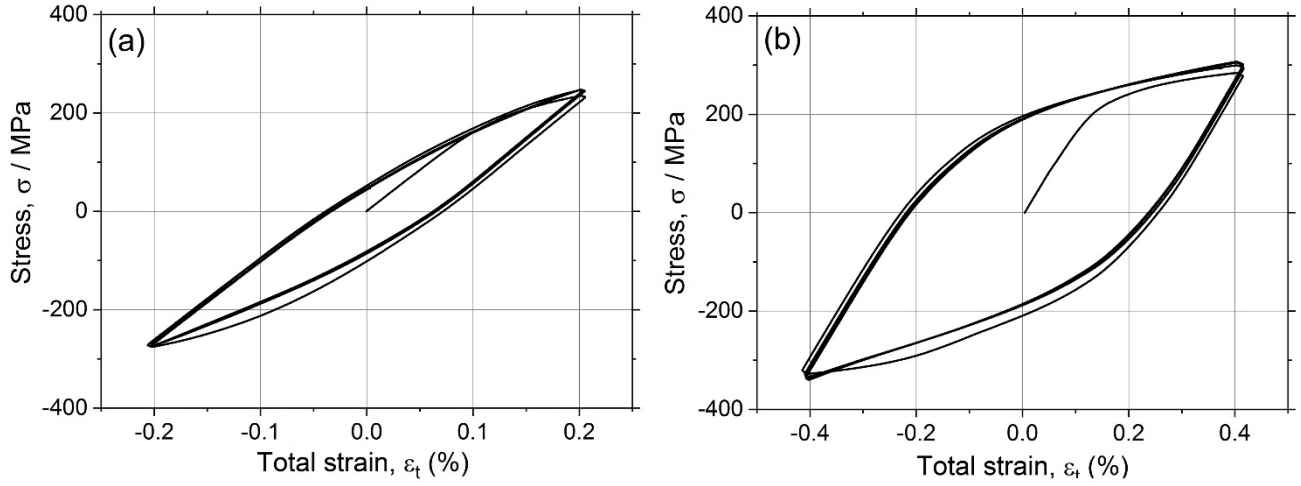

Figure 5. *First five cyclic hysteresis loops obtained in the TiAl alloy under strain-controlled cyclic testing with the total strain amplitude (a)* ε_a = 0.2% *and (b)* 0.4%. *The loading started in the tensile direction.*

When the crosshead of the testing machine controlled by the triangular waveform signal changes the sense of movement, the dislocations continue their forward motion until the sign of the effective acting stress alters. Then, after a short period of elastic straining, the individual micro-volumes start to deform plastically, and plastic deformation proceeds progressively over the entire specimen volume. This results in the curvature of the stress-strain curve, which can be examined in a mechanistic way proposed by Polák and Klensil [42, 43, 45, 46, 48]. Introducing the relative coordinates σ_r and ε_r where the coordinate origin shifts to the minimum stress and plotting the second derivative of the stress σ_r with respect to ε_r versus the "fictive stress" defined as a product of $\varepsilon_r / 2$ E_{ef} [48]:

$f\left(\frac{\varepsilon_r E_{ef}}{2}\right) = -\frac{2}{E_{ef}^2}\frac{\partial^2 \sigma_r}{\partial \varepsilon_r^2}$. This plot is shown for the first selected cycles in Figs. 6a and 6b for ε_a = 0.2% and

$\sigma_r(\varepsilon_r)$, it is zero at the pure linear elastic part of the hysteresis loop. The maximum of $\partial^2\sigma_r/\partial\varepsilon_r^2$ appears when the majority of micro-volumes starts to deform plastically. In both Figs. 6a and 6b this function is zero until of 50 MPa fictive stress, which corresponds to the effective stress for the onset of the dislocation slip. At larger internal stresses, a broad peak is observed. This peak represents the spectrum of internal stresses triggering dislocation motion. The maximum fictive stress is persistently observed around 170 MPa at ε_a = 0.2%, whereas it shifts to about 220 MPa at ε_a = 0.4%. It is important that shortly before the maximum strain, another sharp peak of the $\frac{2}{E_{ef}}\frac{\partial^2\sigma_r}{\partial\varepsilon_r^2}$ function appears. The second peak in the *f* function is most pronounced during the first cycle. It then reduces with the increasing number of cycles, i.e. with the increasing cyclic hardening. Similarly to the results reported by Polák et al. [46], where the bi-modal structure of $-\frac{2}{E_{ef}^2}\frac{\partial^2\sigma_r}{\partial\varepsilon_r^2}$ has been observed in the low carbon steel, there is no quantitative model-based explanation of the observed maximum as yet. In section 3.5, it will be shown that the twinning activity increases with stress and is thus most frequent at high stress just before stress reversal. Presumably, the second peak in the *f*-function can be associated with the complexity of the strain-dependent interplay between dislocations and deformation twins, resulting in tiny changes in the strain hardening behaviour, which are reflected by the $\partial^2\sigma_r/\partial\varepsilon_r^2$ derivative function in the distinctive way, and which are seen in the AE behaviour discussed below. This assumption is backed by the experimental observations in the twinning activity, which is particularly pronounced during the very first loading cycles as will be shown in what follows. Taking this assumption as a working hypothesis, the reason why the second peak disappears quickly at ε_a = 0.4% while it reduces slowly and remains visible at ε_a = 0.2% for the first several cycles can be associated with the more pronounced dislocation-mediated strain hardening effect at the larger strain amplitude, and with the more pronounced detwinning at the smaller strain amplitude.

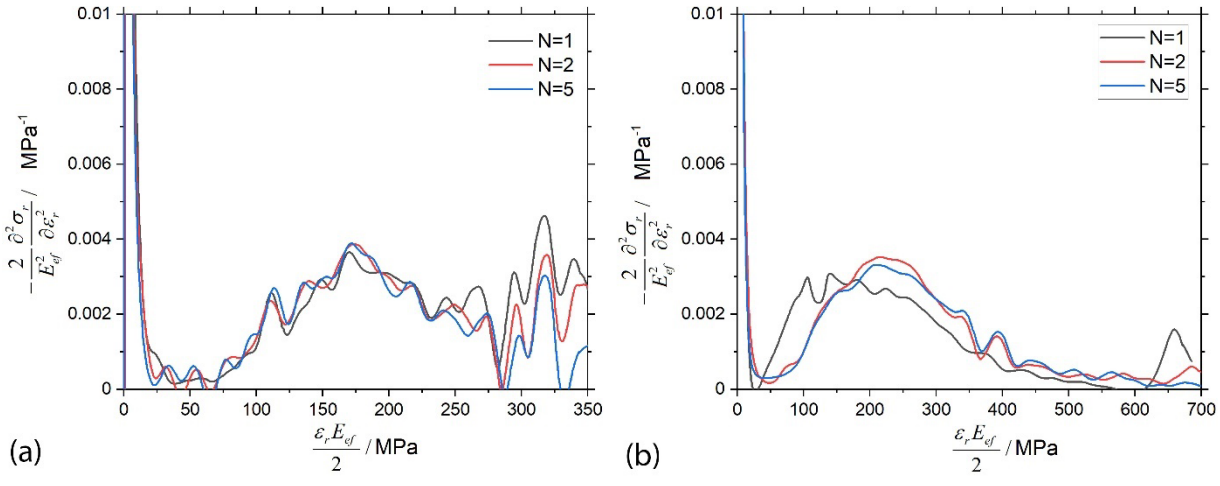

Figure 6. *The second derivative of the ascending part of the hysteresis loop from the minimum to maximum stress: (a)* ε_a = *0.2% and (b)* ε_a = *0.4%.*

3.4 Neutron diffraction

Figure 7 shows the evolution of the lattice strain assessed by neutron diffraction for two families of crystallographic planes - {112} and {110} - upon cycling. It was demonstrated in [12] that deformation twinning along {111} planes creates the tensile stress acting on the {112} planes and the compressive stress acting on the {110} planes. These stresses are developed during the forward loading during the first cycle. They then oscillate in-phase with the loading curve when measured after each tensile or compressive half cycle. This lattice strain behaviour can be interpreted by considering profuse twinning that occurs during the monotonic loading stage, which is then followed by partial detwinning and retwinning during the subsequent half-cycle. The lattice strain after tensile half-cycles increases slightly and saturates after few (e.g. 3-5) cycles. It is interesting to notice that the saturation level is lower for the twinning during compression. According to Skrotzki [16] and Sun et al. [49], for certain grain orientations, twinning cannot take place under compression while it is forbidden under tension for other orientations. Based on their analysis, in the γ-TiAl tetragonal crystal with randomly oriented grains, the formation of twins in tension is more probable than in compression. This is fully corroborated by the results of the AE analysis presented in the following section. In ref. [12], it has been estimated that the detwinning process during compression removes about 20% of the volume of twins formed during the tension half-cycle. This estimate also accounts for the new twins produced in compression. The lattice strain at saturation increases when the total strain amplitude is higher (not shown here, see [12] for details), indicating that more twins are produced in loading at 0.4% when compared to 0.2% strain amplitude.

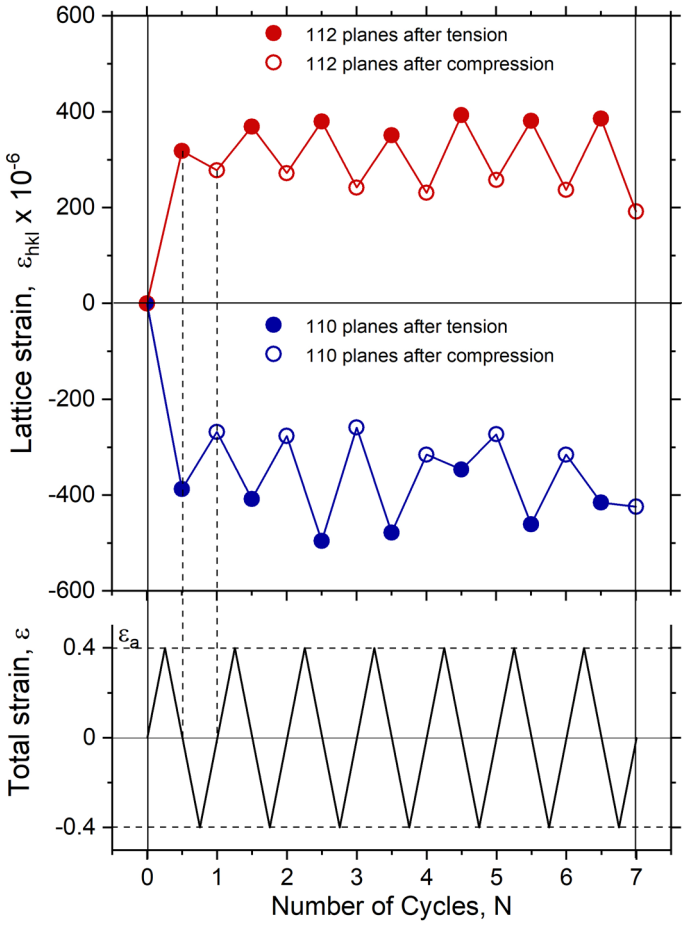

Figure 7. *Evolution of the lattice strain on planes {112} and {110} during cycling with the total strain amplitude* ε_a*=0.4%.*

3.5 Acoustic emission

Figure 8a shows the stress-time diagram superimposed with the raw AE data stream continuously recorded during the four first loading cycles of the TiAl alloy tested at the total strain amplitude 0.2%. As is commonly observed for many ductile metal and alloys and discussed in Introduction, AE commences at the very low applied stress immediately after the beginning of cyclic loading on the first cycle; the signal increases with the applied stress, decreases on unloading and restarts at the stress/strain reversal. As cyclic hardening proceeds, the AE level reduces. In subsequent loading, it tends to reappear at higher stresses due to the Kaiser effect reflecting the irreversibility of AE sources during plastic deformation and/or fracture [20]. Nonetheless, since AE reappears in both loading direction at stresses below those reached in the previous straining session. Hence, the same Kaiser effect strongly suggests that plastic deformation is only partially irreversible. This observation is in excellent agreement with the Bauschinger effect which is commonly seen in metals and alloys under fully reversed loading.

Figure 8b represents a magnified fragment of 8(a), revealing a pattern of intermittent AE signals buried in continuous background noise. One can see that AE appears as a time series of well-separated transients with broadly varying amplitudes, Figs. 8c and d.

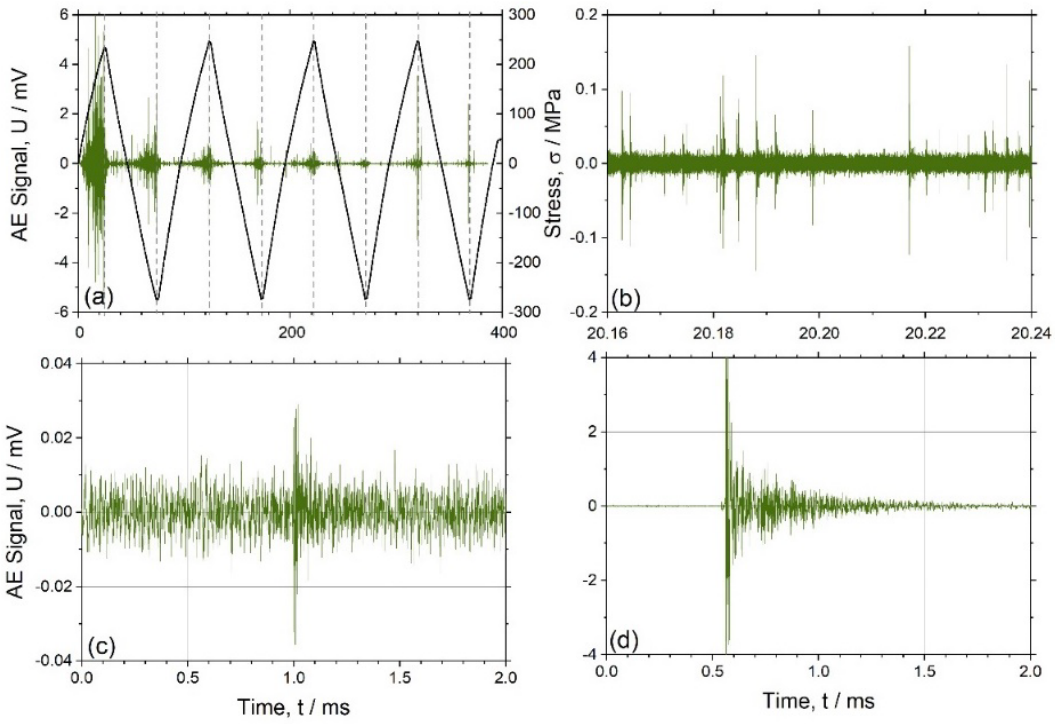

Figure 8. *Raw AE streaming data continuously recorded during four first loading cycles of the TiAl alloy tested at the total strain amplitude* ε_a *=0.2% (a) and its fragments revealing the structure of AE pulse train (b) and two characteristic transient signals with different waveforms and amplitudes buried into background noise (c) and (d).*

Figure 9a illustrates the AE behaviour in the same alloy in terms of the *AE Power* P_{AE} and the median frequency f_m of the PSD function. AE exhibits the behaviour typical of metals and alloys with plastic deformation mediated by two concurrent mechanisms – dislocation slip and twinning; hcp Zn, Mg-alloys [33, 34, 50, 51] and TWIP steels [32, 52] are among the most typical materials of this kind. As is common for many metals and alloys regardless of the type of their crystal lattice, the AE power peaks shortly after plastic yielding in either the tension or compression stage of each cycle. It decays gradually afterwards in response

to cyclic hardening associated with the growing density of dislocations and twins and with the concomitant decrease in the twin length and the dislocation mean free path. The reduction in the dislocation mean free path is reflected by the characteristic behaviour of the AE median frequency that exhibits a clear shift to a high-frequency domain during the uniform strain hardening stage in metals [53].

The tension-compression asymmetry of the hysteresis loops is, in general, not significant in the present experiments, except the very first hysteresis loop Fig. 5. This can be ascribed to the preponderance of twinning in tension over that in compression, which is particularly evident from the neutron diffraction results and is corroborated by AE measurements when comparing the first tension and compression half-cycles and the corresponding AE behaviour in Figs. 8 and 9.

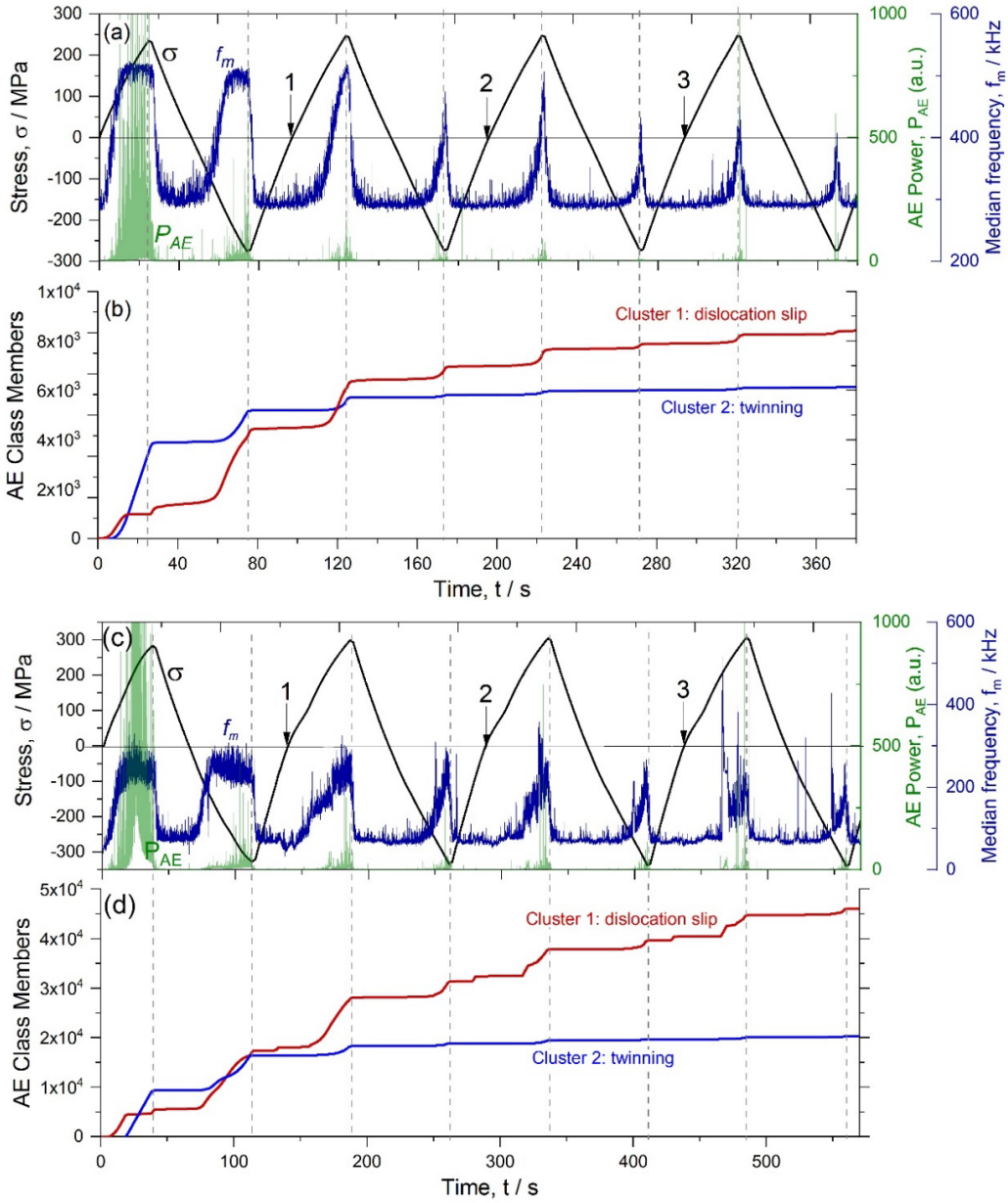

Figure 9. *Loading diagram synchronised with the AE average power P_{AE} and median frequency f_m of the PSD and the corresponding results of the AE cluster analysis for the first loading cycles (the end of each cycle is indicated by the numbered arrow) of the TiAl alloy tested at ε_a =0.2% (a, b) and 0.4% (c,d) ; vertical dashed lines indicate the peaks and valleys of the deformation cycles.*

When compared to dislocation motion, the twinning activity results in the distinctly different AE response exhibiting multiple high amplitude transient signals with short rise time, like that shown in Fig. 8d. The train of such pulses forms a time series with a relatively high activity/count rate, Fig. 8b. Even though the individual AE events can be caused by an avalanche [54] dynamics of multiple dislocation segments moving collectively, overall AE flow generated by dislocation motion during strain hardening of pure metals manifests itself either as a random Poisson-like point process of independent sources [55, 56] or an Ornstein-Uhlenbeck type continuous process with local memory of the past determined by the characteristic relaxation time in the system and interrelated with the AE median frequency [53]. The statistical analysis of transient signals in pure titanium and magnesium and its alloys has shown that, unlike dislocation slip, twinning is a strongly correlated dynamic process with the relatively long memory of preceding events, which is evidenced by a pronounced deviation of AE inter-arrival times from the Poisson's statistics [55, 56]. When the activity of the short transient events is high enough, e.g. due to profuse twinning, the median frequency of the AE PSD saturates due to the limited bandwidth of the AE sensor as can be seen in Fig. 9a close to the peak tensile and compressive stress during the first loading cycle where the f_m value levels out. Such an AE behaviour is very similar to what is frequently observed in plastically deformed magnesium alloys [33] or TWIP steels [32], where mechanical twinning represents a fundamental deformation mode. It, however, differs drastically from AE generated by dislocation motion in pure fcc and bcc metals. Since individual mechanical twins behave similarly in terms of their dynamics during nucleation and propagation, the AE PSD does not evolve when plastic deformation is governed by twinning, and the f_m value tends to level out at a relatively high value. However, when the dislocation slip prevails, the AE power spectrum progressively shifts to higher frequencies with the increasing strain. This kind of behaviour of the AE spectrum has been commonly documented for many pure fcc metals (e.g. copper, aluminium, nickel) and alloys (e.g. stainless steel, α-brass) [29, 57, 58]. The dislocation slip in pure fcc metals is accompanied by continuous noise-like AE of relatively small amplitude, which reduces progressively with strain hardening due to dislocation accumulation and the increasing friction for dislocation motion [53, 58-60]. The reduction in the dislocation mean free path with increasing strain gives rise to the steadily growing AE median frequency, i.e. to the shift of the AE spectrum to the higher frequency domain – the effect, which has long been recognised in the dislocation-mediated plasticity [53, 57, 61], and which is seen systematically in all loading fragments shown in Fig. 9 when the load crosses zero and increases in either tensile or compressive direction.

As the direction of loading changes at peak stresses, the AE activity decreases almost to zero, and the AE median frequency drops to its initial value corresponding to the background noise. Clearly, the overall AE activity reduces progressively with the number of cycles due to cyclic hardening as it is reasonably expected from the commonly observed trends in the AE behaviour during monotonic [20] or cyclic plastic deformation of metals [62]. The profuse mechanical twinning is particularly evident during the first loading cycle in both tension and compression. When the direction of loading reverses from tension to compression, the twinning activity recorded during the second half of the loading cycle is lower compared to that during the first half-cycle. This, however, does not reflect any tension-compression asymmetry since, as has been noticed above, the behaviour of both the cyclic hysteresis loop and AE appeared to be independent of the direction of the first loading. Rather, the difference in the AE behaviour during the first and the second half-cycles is logically related to the irreversibility of the cyclic hardening process associated with the above-discussed Kaiser effect.

Although the twinning activity notably reduces with cycling, it does not vanish entirely within the cyclic history observed. These conclusions are strongly corroborated by the AE cluster analysis. The non-supervised ASK algorithm distinguished between two major types of AE signals, which differ from noise and which have statistically different shapes of the power spectral densities (we should recall here that the ASK procedure is data-driven, and it does not require the number of deriving clusters to be specified *a priori*). Main findings of the cluster analysis in the TiAl alloy are summarised in Figs. 9b and d for both strain

amplitudes used in the tests. The twinning activity is notably higher in the specimen deformed at larger (0.4%) strain amplitude, which is in harmony with microscopic observations. The trend towards saturation is clearly visualised for the twinning sub-system.

Centroids of the identified major clusters are shown in Fig. 10a in terms of the normalised mean PSD functions exhibiting notably different contributions from low- and high-frequency components. Figure 10b illustrates the same finding in the U_p - f_m coordinates where a reasonably good separation between the AE clusters is also observed (we should notice here that this scatter plot is made for illustrative purposes solely; the signal clustering has been performed by comparing the PSD functions as described in [30]). The signals from both contributing mechanisms – dislocation slip and twinning - often overlap in time. They also share the same frequency domain due to the resonances pronounced in the frequency response of the sensor. Nevertheless, the signals associated with twins systematically appear with the notably higher amplitude than those from the dislocation sources. It should be noted that the present AE experimental setup does not make it possible to discriminate between the motion of the ordinary dislocations and superdislocations despite the difference in their geometry and details of their motion. The amplitude distributions of the transients from the twin-related AE cluster can be approximated by the log-normal model (not shown here) resembling the grain size distribution shown in Fig. 1c, c.f. [33], as has been argued in [21] on the basis of the linear elastodynamic AE source model proposed in [63].

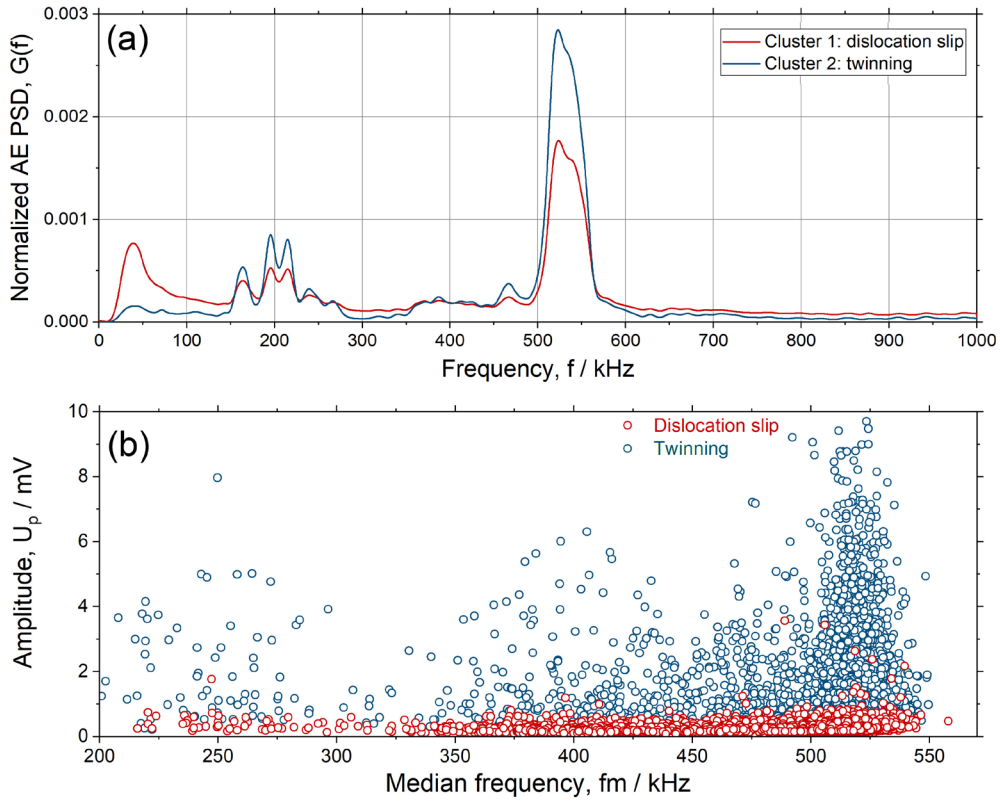

Figure 10. *Results of discrimination between different AE clusters distinguished by the shapes of their normalised PSD functions in the TiAl alloy tested at ε_a =0.2%; Centroids of clusters (a) and the bi-variate distribution of AE amplitudes U_p vs median frequencies f_m of the PSD (b). The pronounced resonance at 520 kHz in (a) corresponds to that in the sensor frequency response.*

Evolution of both clusters with cyclic deformation can be seen in Fig. 9b and d in terms of the number of elements belonging to two different clusters associated with dislocation slip and twinning.

Interestingly, the AE cluster analysis witnesses that dislocation slip dominates the initial strain hardening rate. However, mechanical twinning sets in shortly after yielding, and the crossover between the contributions from two mechanisms occurs at about 15 s as is seen in Fig. 9b (see also Fig. 9d). Hence, the rest of the deformation process at ε_a=0.2% during the first loading cycle is dominated by twinning (this is not exactly the same at ε_a=0.4% as will be discussed below). The mechanical twins nucleate in both tension and compression, albeit admittedly with different rates (the twinning progresses more rapidly in tension than in the following compression). As cycling proceeds, the rate of twinning reduces, and the twinning process shows a clear tendency towards saturation. Nonetheless, the dislocation activity remains recognisable in the AE signal despite the significantly decreasing power due to strain hardening and the concomitant shortening of the dislocation free path. Although the twinning activity does not vanish until the end of the test, it reduces by orders of magnitude. Therefore, using the cumulative AE power or the cumulative number of AE events in the twinning-related class of signals, it is safe to estimate the twin fraction of 84 % after the first cycle and 95% after the second regardless of the applied strain amplitude (100% twin fraction is assumed to be corresponding to the end of the test; this should not be confused with the twin volume fraction, which is not known from the indirect AE measurements even though the latter can be calibrated by using the microstructural quantitative assessment of the twin density).

4. Discussion

Before commencing the discussion on the primary findings of the present study, it is timely to recall that the influence of the microstructure on mechanical properties and deformation mechanisms in TiAl alloys has long been studied and frequently reported [1, 2, 4-11, 16, 64-67]. Most of the cited results were obtained either in uniaxial tension (compression) or creep testing, and, to a much lesser extent, under cyclic deformation. The $L1_0$ ordered structure of the γ-TiAl phase is face centered tetragonal (fct) with the *c* axis longer than the *a* axis by few percent [68]. In this structure, Ti and Al atoms form alternating layers parallel to the (001) planes. According to the commonly accepted scenario, plasticity in the γ-TiAl phase involves a combined behaviour of three primary modes: (i) slip of ordinary ½ <110] dislocations with the zero *z* component of the Burgers vector, (ii) slip of <101] superdislocations, and (iii) mechanical twinning. The last two deformation modes are supposed to need a higher critical shear stress to get activated if compared to slip of the ordinary dislocations [67]. Therefore, the dislocation structure in the Ti-48Al based alloys [1, 2, 4-12, 64] is largely dominated by unit ½ <110] dislocations even in the grains with lower Schmid factors, whereas <101] superdislocation slip occurs also in favorably orientated grains. However, even the slip of ordinary ½ <110] dislocations does not occur smoothly. Screw dislocations are often observed to be pinned by local obstacles, the density of which increases with temperature. It leads to the high work-hardening rate, and even to a temperature anomaly of the flow stress [69]. The essential role played by twinning in the mechanical response of these alloys has been emphasized on many occasions (see, for example, [12, 16, 17, 65, 67]). The common conclusion drawn is that the preponderance of this mechanism is dictated by the Schmid factor in a specific grain [16, 67]. The two-fold role of twins in the deformation processes occurring in TiAl alloys is widely discussed in the literature in conjunction with two major effects: on the one hand the twins serve as obstacles for dislocation/superdislocation slip causing the higher hardening rate and promoting brittle fracture, while on the other hand they provide an extra mode of plastic accommodation, fulfilling the von Mises plasticity criterion. Although the consensus has been reached in the literature on many aspects of plasticity of TiAl alloys, the controversies still remain unsolved regarding the mutual interplay between deformation twinning and dislocation slip, the significance of twinning in the cyclic hardening and fracture [1][10][16, 26-28]. In this sense, the critical assessment of the spectral and statistical features of acoustic emissions bearing their origin in primary deformation modes provides a real-time (albeit

indirect) access to the kinetics of deformation mechanisms underlying the cyclic hardening process. Powered and supported by independent direct microstructural observations, the AE results offer new insight into the activity of established operating mechanisms - dislocation slip, twinning and detwinning – in cyclic deformation.

First and foremost, it is instructive to notice that the AE behaviour in the TiAl alloy differs drastically from that in pure fcc metals where plasticity is mediated solely by dislocation mechanisms. Figure 11 shows, as a typical example, the AE power evolving during cyclic deformation of a textureless 99.98% polycrystalline copper specimen annealed at 850°C for 1 h and cyclically tested under the same conditions at ε_a =0.2%. The fragment of the AE stream shown in Fig. 11a represents the AE signal during plastic deformation of pure copper. AE is seen as a continuous random noise-like signal, which, however, should not be confused with the background electrical noise since it was recorded between 9 and 10 s of deformation when AE is notably higher than the noise level. The ASK algorithm easily distinguishes between AE and noise (Fig. 11c). No other deformation processes have been identified at this stage of fatigue, and the dislocation slip represents the sole active deformation mechanism. The continuous AE waveform characteristic of dislocation slip differs strikingly from the transients caused by twinning in TiAl. Most importantly for the context of the present work, is that as soon as the direction of loading reverses at peak tensile or compressive loads, the AE immediately drops to the background level as illustrated in Fig. 11b and c, and only background noise is recorded until plastic yielding restarts again. This is evidently seen in Fig. 11c. Thus, the unloading begins as a purely elastic process that is reasonably expected for most structural materials with dislocation-mediated plasticity.

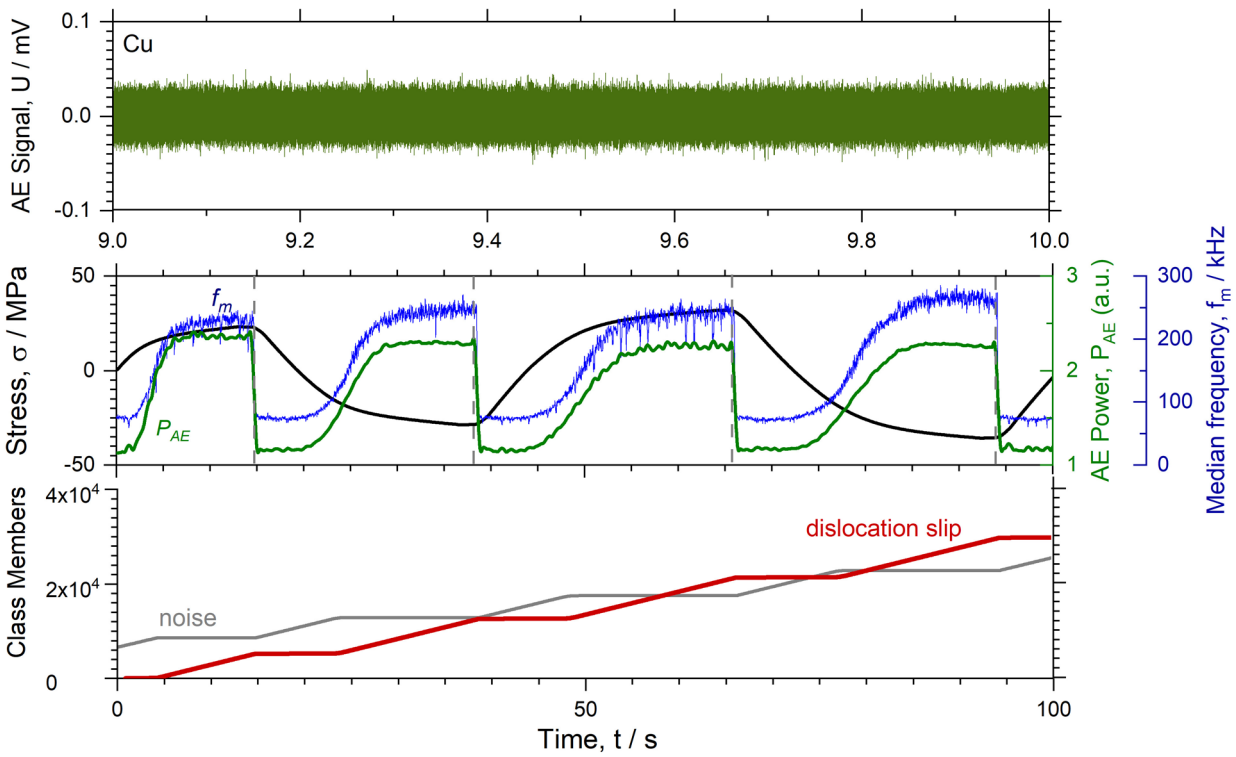

Figure 11. *Fragment of the continuous recording of the AE signal in a pure copper polycrystalline specimen cyclically tested under the same conditions as the TiAl alloy for comparison; (a) realisation of the raw signal of 1 s duration; (b) the average AE power and the median frequency are plotted together with the loading diagram; (c) shows the result of the ASK cluster analysis revealing only one AE cluster which is distinguished from noise (the result for background noise is also plotted for comparison).*

The behaviour of the TiAl alloy is fundamentally different as can be best seen in the enlarged fragments of the AE data representing the first loading cycle, Fig. 12. Importantly is that in the TiAl alloy AE does not drop sharply at the points of load reversal (as opposes to that in Cu). Instead, it gradually decays to the background level as the stress decreases. One can notice that just beyond the first load reversal, AE retains some high amplitude transients. However, the ASK clustering analysis unambiguously suggests that these bursts are not related to twins and should be ascribed to the dislocation-like mechanisms according to their spectral features. This is witnessed by the increasing activity of the dislocation-related AE cluster in Fig. 12a in the grey-shaded area. Comparing the results obtained on the specimens tested at ε_a =0.2% (Fig. 12a) and 0.4% (Fig. 12b), one can notice that besides the apparent similarity between the two, there is an essential difference in the unloading behaviour: (i) the specimens tested at lower strain amplitude 0.2% show the considerably higher AE activity and (ii) the slower decrease in the AE signal upon changing the direction of loading than the specimens tested at ε_a=0.4%. This occurs despite the notable difference in the overall AE activity, which is expectedly higher in the specimens tested at ε_a =0.4% due to the longer uploading time to the higher strains and stresses. We should also notice that the twin-related cluster remains practically inactive during the unloading stage until yielding resumes under compressive stresses in the second half-cycle. Concurrently, after the reappearance in compression, twinning is more active in the specimen tested at ε_a=0.2% than at ε_a=0.4%. Thus, concluding this section, the signatures of AE observed at the stress reversal are indicative of the detwinning process, which occurs in the alloy studied and which bears notable similarity to the anelasticity and detwinning behaviour in Mg alloys [50, 51, 70]. This process occurs appreciably differently from preceding twinning as reflected by the fluctuating behaviour of the dislocation-mediated acoustic emission, and it is more pronounced at lower strain amplitudes. This result appears to be entirely in line with the microscopic findings showing the significantly higher density of both dislocations and micro-twins in the specimens tested at larger ε_a (see Fig. 3 and ref. [12]). The significant difference visible between the few twins found after testing at ε_a =0.2% and large colonies of twins observed after testing at ε_a=0.4% is plausibly rationalised in terms of the AE results. The detwinning occurs more easily on reversal after loading to smaller strains. Indeed, the AE behaviour evidences ubiquitously that both twinning and dislocation slip coexist during the strain hardening process. The dislocations stored in the grains interact with twin boundaries, anchor them and impede detwinning. This scenario is obviously more pronounced at higher strain amplitude. Once detwinning occurs, the density of twins reduces, and retwinning is highly possible, accounting for the relatively higher activity of the AE twin-associated cluster in compression of the specimen tested at ε_a =0.2%. At the larger strain amplitude, the dislocation activity is greater (c.f. Fig. 12a and b, and the supporting microstructural details in ref. [12]) and the twin boundaries are strongly pinned by dislocations stored in the grains. This impedes the detwinning process and accounts for the sharper drop of the AE level observed upon changing the direction of loading if compared to that at lower strain amplitude ε_a =0.2%. Thus, an important corollary from the AE observations is that detwinning plays an essential role in the kinetics of twin accumulation, and it is the rate of dislocation accumulation, which controls this process.

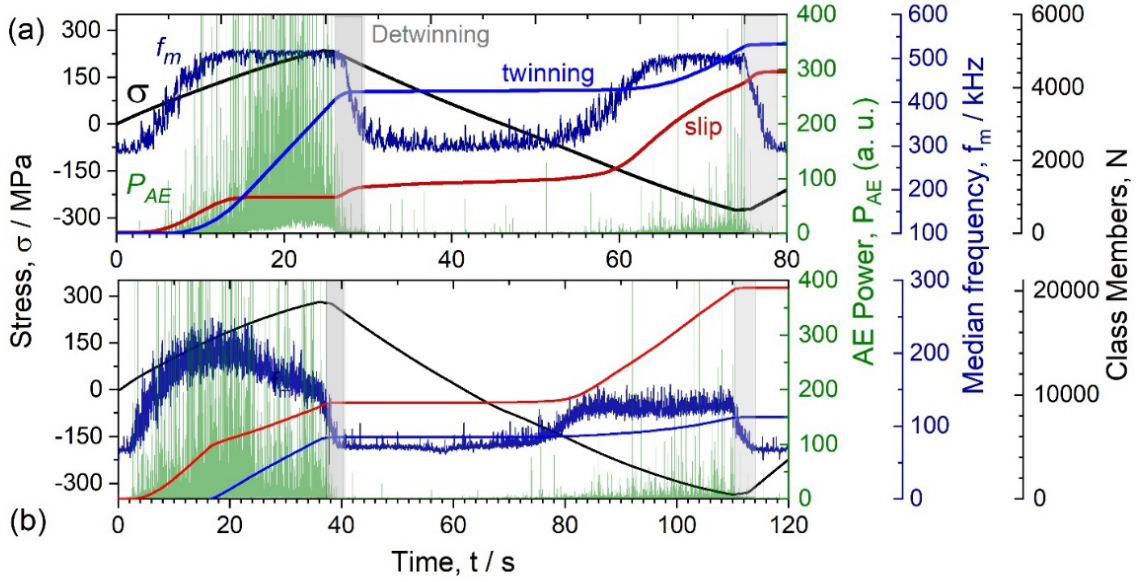

Figure 12. *Enlarged fragments of AE streaming data acquired during the first loading cycle in the TiAl alloy tested at the total strain amplitude ε_a =0.2% (a) and 0.4% (b).*

The occurrence of partial detwinning upon load reversal is witnessed collectively by neutron diffraction and AE methods. The detwinning process is more pronounced at the lower strain amplitude due to the lower dislocation contribution to the strain hardening as dislocations can pin the twin boundaries and impede detwinning when the sense of loading changes. The detwinning process is supposed to be important for local stress relaxation and extension of fatigue life.

The present findings provide new insight into the nature of the rapid initial cyclic hardening reported in [12]. The sharp increase in the cyclic stress amplitude during the first strain-controlled loading cycles correlates with profuse mechanical twinning, which tends to saturate after few cycles, and the further cyclic hardening is governed by the evolution of the dislocation sub-system. The twin lamellae extending from one grain boundary to another do not exert a significant hardening effect since their volume fraction is relatively small, and they do not create strong long-range stress fields in the crystal lattice. However, the dynamic Hall-Petch effect [71, 72] arising in response to the dislocation-twin interactions can be the root cause for the rapid cyclic hardening observed: the mechanical twins act as obstacles to dislocation motion, promoting the formation of dislocation bundles. Thus, the greater twin density, which is seen at the larger strain amplitude, results in a more pronounced strain hardening.

Besides, it is interesting to notice that while the AE PSD shifts to a higher frequency domain during either tensile or compressive part of each loading cycle as has been discussed above, the maximum f_m value achieved during each loading session decreases with the number of cycles, c.f. Figs. 8 and 9. This finding also contrasts with what is typically seen in metals where dislocation glide is the sole deformation mechanism and where the maximum f_m value increases in each cycle in response to the shortening of the dislocation mean free path with cyclic hardening 62]. Figure 11 nicely illustrates this common PSD trend on the example of polycrystalline copper. The observed specific AE PSD behaviour in the TiAl alloy, which is reflected by the median frequency, is apparently related to the effect of twinning operating concurrently with dislocation slip. Indeed, throughout the deformation process these two deformation modes coexist contributing collectively to the resultant AE. There is no particular “point” of sharp transition between these mechanisms. Within any single realisation of 2 ms (4096 readings), the AE flux contains the signatures of both mechanisms. Compared to dislocation slip, twinning excites the AE sensor at higher frequencies, c.f. Fig. 10, and, therefore, provides the major contribution to the high frequency components of the PSD. As the

twinning activity reduces quickly with cycling and the relative contribution of dislocation slip increases accordingly, the maximum median frequency per half-cycle decreases too as it is seen in Figs. 8 and 9, overriding the opposite trend in the f_m behaviour anticipated due to dislocation accumulation in the grains.

The significance of twinning in brittle fracture of single phase TiAl alloys has been emphasised in [73] (c.f. also [74, 75]). The low ductility and the propensity to cleavage of titanium-aluminides was attributed to a combined effect of the low mobility of slip and twin dislocations and the relatively low cleavage strength. Considering the high sensitivity of TiAl alloys to small fatigue cracks [76], understanding the role of the microstructure and the underlying deformation mechanisms in fatigue crack initiation is crucial for potential structural applications. As a matter of discussion, we suppose that, given the known capacity of the advanced AE technique to discriminate between twinning, dislocation slip and microcrack initiation [33], the methodological approach proposed in the present paper might be useful to rationalise the role of mechanical twins in the cyclic crack initiation, which has been a subject of debates in the recent past. On the one hand, in cyclically deformed near-γ TiAl, microcrack initiation has been frequently observed due to interactions between deformation-induced twins and grain boundaries [77-79] (the mechanisms controlling the effects of twin-slip interaction on the fatigue crack initiation and growth are still unclear and require further study). On the other hand, the present results demonstrate unequivocally that the twins nucleate primarily during the very early stage of cyclic hardening when no cracks are observed. As it was shown above, the twin activity reduces with cycling, giving way to dislocation mechanisms operating throughout the entire fatigue life until the crack sets in. The dislocation-mediated strain hardening processes (i) impede detwinning – the important stress-relieving mechanism, which is clearly seen by both neutron diffraction and AE methods, and which is more significant at the smaller strain amplitude, and (ii) increase the local stresses. Both these processes adversely affect fatigue life. Since the twin shear accommodation at grain boundaries leaves residual defects in the boundary [77], the highly stressed intersections between the impinged twins and grain boundaries become particularly vulnerable to crack initiation. Although we were focused on the early stage of fatigue and did not investigate the crack initiation and propagation behaviour in the present study (this can be a scope of the further work), the proposed scenario seems to be well supported by the findings of the present work.

5. Summary

Motivated by the need for a better understanding of the deformation mechanisms underlying the cyclic response of the near γ-TiAl alloy, we unveiled the relative contributions of the primary deformation mechanisms - slip of ordinary dislocations/superdislocations and mechanical twinning - using a rare blend of advanced characterisation techniques involving *ex situ* TEM and SEM–ECCI/EBSD microstructural examinations complemented by *in-situ* neutron diffraction and acoustic emission measurements. The mechanical response was described by the analysis of the hysteresis loops, which was correlated with changes in the microstructure due to mechanical twinning, dislocation slip and detwinning. The broadband AE technique powered by the advanced signal clustering analysis was shown to be well-suited to discriminating between twinning and dislocation slip in the γ-TiAl alloy, even when these mechanisms were operating concurrently during the cyclic test. Based on this experimental effort, the description of the microstructure evolution and the operating plasticity mechanisms could be traced both within individual cycles and throughout the whole fatigue life:

1. Both dislocation slip and twinning operate throughout the entire cyclic deformation process, although their contributions to strain hardening and the AE response are different, depending on the applied strain amplitude and the number of loading cycles.

2. Microscopic observations convincingly show that the cyclic deformation leads to the production and accumulation of both dislocations and the deformation twins. The amount of dislocations and

mechanical twins is higher at higher strain amplitude. The thickness of deformation-induced twins in this alloy vary between 15 and 35 nm depending on grain size and orientation.

3. The cluster analysis of AE spectra shows that although cyclic plastic deformation commences with ordinary dislocation slip, twinning appears as a prevailing deformation mode in the first loading cycle for both 0.2% and 0.4% total strain amplitudes. This is also supported by neutron diffraction and electron microscopy.

4. Within each cycle, the dislocation slip precedes twinning. The twinning activity accelerates with stress. The reversal of loading is followed by detwinning amounting to of 20% of the twinned volume.

5. The twinning activity reduces sharply after the first loading cycle, although it does not vanish at least during the first five loading cycles examined; as twinning tends to saturate, the dislocation slip becomes the governing mechanism of cyclic plastic deformation.

6. The evolution of the lattice strain assessed by ND in the course of cyclic loading showed that the most significant increase of the lattice strain occurs in the first cycle where the twinning process is also most pronounced according to the results from both independent AE measurements. The rate of the lattice strain evolution reduces after a few first cycles concomitantly with the reduction of the activity of twins.

Acknowledgements.

Electron microscopy investigations were partly performed using facilities of the CEITEC Nano Research Infrastructure (ID LM2015041, MEYS CR, 2016-2019). Support is also acknowledged from the Thermo Fisher Scientific & Czechoslovak Microscopy Society fellowship awarded to Milan Heczko. Authors would like to thank Dagmar Herzánová for preparation of twin-jet foils for TEM. T.K. gratefully acknowledges the financial support provided by the Ministry of Education, Youth and Sports of the Czech Republic within the research project 'Architectured materials designed for additive manufacturing', No.: CZ.02.1.01/0.0/0.0/16_025/0007304.

6. REFERENCES

[1] F. Appel, J.D.H. Paul, M. Oehring, Gamma titanium aluminide alloys science and technology, Wiley, Weinheim, 2011.
[2] X.H. Wu, Review of alloy and process development of TiAl alloys, Intermetallics 14(10-11) (2006) 1114-1122.
[3] T.E.J. Edwards, F. Di Gioacchino, G. Mohanty, J. Wehrs, J. Michler, W.J. Clegg, Longitudinal twinning in a TiAl alloy at high temperature by in situ microcompression, Acta Materialia 148 (2018) 202-215.
[4] A. Brotzu, F. Felli, F. Marra, D. Pilone, G. Pulci, Mechanical properties of a TiAl-based alloy at room and high temperatures, Materials Science and Technology 34(15) (2018) 1847-1853.
[5] A. Chlupová, M. Heczko, K. Obrtlík, J. Polák, P. Roupcová, P. Beran, T. Kruml, Mechanical properties of high niobium TiAl alloys doped with Mo and C, Materials & Design 99 (2016) 284-292.
[6] B.P. Bewlay, S. Nag, A. Suzuki, M.J. Weimer, TiAl alloys in commercial aircraft engines, Materials at High Temperatures 33(4-5) (2016) 549-559.
[7] H. Clemens, S. Mayer, Design, Processing, Microstructure, Properties, and Applications of Advanced Intermetallic TiAl Alloys, Advanced Engineering Materials 15(4) (2013) 191-215.

[8] H.Y. Yasuda, T. Nakano, Y. Umakoshi, Cyclic deformation behaviour of Ti-Al alloys containing oriented lamellae, Philosophical Magazine A 71(1) (1995) 127-138.
[9] Y. Umakoshi, H.Y. Yasuda, T. Nakano, Plastic anisotropy and fatigue of TiAl PST crystals: a review, Intermetallics 4 (1996) S65-S75.
[10] G. Hénaff, A.L. Gloanec, Fatigue properties of TiAl alloys, Intermetallics 13(5) (2005) 543-558.
[11] G.B. Viswanathan, M.J. Mills, V.K. Vasudevan, Microstructural effects on the tensile properties and deformation behavior of a Ti-48Al gamma titanium aluminide, Metallurgical and Materials Transactions A 34A(10) (2003) 2113-2127.
[12] P. Beran, M. Heczko, T. Kruml, T. Panzner, S. van Petegem, Complex investigation of deformation twinning in γ-TiAl by TEM and neutron diffraction, Journal of the Mechanics and Physics of Solids 95 (2016) 647-662.
[13] R. von Mises, Mechanik der plastichen Formänderung von Kristallen, Matematik und Mechanik 8 (1928) 161-185.
[14] F.D. Fischer, T. Schaden, F. Appel, H. Clemens, Mechanical twins, their development and growth, European Journal of Mechanics - A/Solids 22(5) (2003) 709-726.
[15] W.T. Marketz, F.D. Fischer, H. Clemens, Deformation mechanisms in TiAl intermetallics—experiments and modeling, International Journal of Plasticity 19(3) (2003) 281-321.
[16] B. Skrotzki, Crystallographic aspects of deformation twinning and consequences for plastic deformation processes in γ-TiAl, Acta Materialia 48(4) (2000) 851-862.
[17] H. Tanaka, R. Horiuchi, Acoustic-Emission Due to Deformation Twinning in Titanium and Ti-6a1-4v Alloy, Scripta Metallurgica 9(7) (1975) 777-780.
[18] F. Kauffmann, T. Bidlingmaier, G. Dehm, A. Wanner, H. Clemens, On the origin of acoustic emission during room temperature compressive deformation of a γ-TiAl based alloy, Intermetallics 8(7) (2000) 823-830.
[19] W.T. Marketz, F.D. Fischer, F. Kauffmann, G. Dehm, T. Bidlingmaier, A. Wanner, H. Clemens, On the role of twinning during room temperature deformation of γ-TiAl based alloys, Materials Science and Engineering: A 329-331 (2002) 177-183.
[20] C.R. Heiple, S.H. Carpenter, Acoustic Emission Produced by Deformation of Metals and Alloys - A review: Part I and II, J. Acoustic Emission. 6(3) (1987) 177-237.
[21] A. Vinogradov, E. Vasilev, M. Seleznev, K. Máthis, D. Orlov, D. Merson, On the limits of acoustic emission detectability for twinning, Materials Letters 183 (2016) 417-419.
[22] R. Botten, X. Wu, D. Hu, M.H. Loretto, The significance of acoustic emission during stressing of TiAl-based alloys. Part I: Detection of cracking during loading up in tension, Acta Materialia 49(10) (2001) 1687-1691.
[23] X. Wu, D. Hu, R. Botten, M.H. Loretto, The significance of acoustic emission during stressing of TiAl-based alloys. Part II: Influence of cracks induced by pre-stressing on the fatigue life, Acta Materialia 49(10) (2001) 1693-1699.
[24] D. Hu, A. Huang, H. Jiang, N. Mota-Solis, X. Wu, Pre-yielding and pre-yield cracking in TiAl-based alloys, Intermetallics 14(1) (2006) 82-90.
[25] G. Lütjering, J.C. Williams, A. Gysler, Microstructure and mechanical properties of titanium alloys, Microstructure and Properties of Materials, WORLD SCIENTIFIC2000, pp. 1-77.
[26] D.Y. Seo, T.R. Bieler, D.E. Larsen, Effect of stress and temperature on primary creep of Ti-47Al-2Nb-1Mn-0.5W-0.5Mo-0.2Si alloy, in: J.C. Earthman, F.A. Mohamed (Eds.) Minerals, Metals & Materials Soc (TMS), Warrendale, PA, United States, 1997, pp. 577-586.
[27] M.A. Morris, T. Lipe, I. Creep deformation of duplex and lamellar TiAl alloys, Intermetallics 5(5) (1997) 329-337.
[28] M.A. Morris, M. Leboeuf, Quantitative analysis of microstructures produced by creep of Ti–48Al–2Cr–2Nb–1B: Thermal and athermal mechanisms, Journal of Materials Research 13(3) (2011) 625-639.
[29] D. Rouby, P. Fleischmann, Spectral Analysis of Acoustic-Emission from Aluminum Single-Crystals Undergoing Plastic-Deformation, Physica Status Solidi a-Applied Research 48(2) (1978) 439-445.
[30] E. Pomponi, A. Vinogradov, A real-time approach to acoustic emission clustering, Mech. Syst. Signal Proc. 40(2) (2013) 791-804.

[31] H.N.G. Wadley, C.B. Scruby, J.E. Sinclair, Acoustic emission source characterization, The Journal of the Acoustical Society of America 68(S1) (1980) S103-S104.
[32] A. Vinogradov, A. Lazarev, M. Linderov, A. Weidner, H. Biermann, Kinetics of deformation processes in high-alloyed cast transformation-induced plasticity/twinning-induced plasticity steels determined by acoustic emission and scanning electron microscopy: Influence of austenite stability on deformation mechanisms, Acta Materialia 61(7) (2013) 2434-2449.
[33] A. Vinogradov, D. Orlov, A. Danyuk, Y. Estrin, Effect of grain size on the mechanisms of plastic deformation in wrought Mg–Zn–Zr alloy revealed by acoustic emission measurements, Acta Materialia 61(6) (2013) 2044-2056.
[34] A. Vinogradov, D. Orlov, A. Danyuk, Y. Estrin, Deformation mechanisms underlying tension–compression asymmetry in magnesium alloy ZK60 revealed by acoustic emission monitoring, Materials Science and Engineering: A 621 (2015) 243-251.
[35] P. Beran, M. Petrenec, M. Heczko, B. Smetana, M. Žaludová, M. Šmíd, T. Kruml, L. Keller, In-situ neutron diffraction study of thermal phase stability in a γ-TiAl based alloy doped with Mo and/or C, Intermetallics 54 (2014) 28-38.
[36] M.J. Blackburn, Some aspects of phase transformations in titanium alloys, in: R.I. Jaffee, N.E. Promisel (Eds.), The Science, Technology and Application of Titanium, Pergamon1970, pp. 633-643.
[37] S.-C. Huang, E.L. Hall, The effects of Cr additions to binary TiAl-base alloys, Metallurgical Transactions A 22(11) (1991) 2619-2627.
[38] P.J. Phillips, M. De Graef, L. Kovarik, A. Agrawal, W. Windl, M.J. Mills, Atomic-resolution defect contrast in low angle annular dark-field STEM, Ultramicroscopy 116 (2012) 47-55.
[39] T.M. Smith, M.S. Hooshmand, B.D. Esser, F. Otto, D.W. McComb, E.P. George, M. Ghazisaeidi, M.J. Mills, Atomic-scale characterization and modeling of 60° dislocations in a high-entropy alloy, Acta Materialia 110 (2016) 352-363.
[40] V.A. Vorontsov, L. Kovarik, M.J. Mills, C.M.F. Rae, High-resolution electron microscopy of dislocation ribbons in a CMSX-4 superalloy single crystal, Acta Materialia 60(12) (2012) 4866-4878.
[41] T.S. Srivatsan, W.O. Soboyejo, M. Strangwood, Cyclic fatigue and fracture behavior of a gamma-titanium aluminide intermetallic, Eng. Fract. Mech. 52(1) (1995) 107-120.
[42] A.L. Gloanec, M. Jouiad, D. Bertheau, M. Grange, G. Hénaff, Low-cycle fatigue and deformation substructures in an engineering TiAl alloy, Intermetallics 15(4) (2007) 520-531.
[43] M. Satoh, S. Horibe, M. Nakamura, H. Uchida, Cyclic deformation and fatigue in TiAl intermetallic compound under plastic strain control, Int. J. Fatigue 32(4) (2010) 698-702.
[44] P. Serrano, L. Toualbi, P. Kanoute, A. Couret, Cyclic deformation of TiAl generic microstructures at room and high temperature: Bauschinger effect & strain rate sensitivity, Intermetallics 122 (2020) 106816.
[45] J. Polák, M. Klesnil, The hysteresis loop 1. A statistical theory, Fatigue & Fracture of Engineering Materials & Structures 5(1) (1982) 19-32.
[46] J. Polák, M. Klesnil, J. Helešic, The hysteresis loop 2. An analysis of the loop shape, Fatigue & Fracture of Engineering Materials & Structures 5(1) (1982) 33-44.
[47] G. Masing, Zur Heynschen Theorie der Verfestigung der Metalle durch verborgene elastische Spannungen, Wissenschaftliche Veröffentlichung aus dem Siemens-Konzern Wissenschaftliche Veröffentlichung aus dem Siemens-Konzern 3 (1923) 231-239.
[48] J. Polak, I. Milne, R.O. Ritchie, B. Karihaloo, Cyclic Deformation, Crack Initiation, and Low-cycle Fatigue, Comprehensive Structural Integrity, Pergamon, Oxford, 2003, pp. 1-39.
[49] Y.Q. Sun, P.M. Hazzledine, J.W. Christian, Intersections of deformation twins in TiAl, Philosophical Magazine A 68(3) (1993) 471-494.
[50] D. Drozdenko, J. Bohlen, S. Yi, P. Minárik, F. Chmelík, P. Dobroň, Investigating a twinning–detwinning process in wrought Mg alloys by the acoustic emission technique, Acta Materialia 110 (2016) 103-113.
[51] A. Vinogradov, E. Vasilev, M. Linderov, D. Merson, In situ observations of the kinetics of twinning–detwinning and dislocation slip in magnesium, Materials Science and Engineering: A 676 (2016) 351-360.
[52] M. Linderov, C. Segel, A. Weidner, H. Biermann, A. Vinogradov, Deformation mechanisms in austenitic TRIP/TWIP steels at room and elevated temperature investigated by acoustic emission and scanning electron microscopy, Materials Science and Engineering A 597 (2014) 183-193.

[53] A. Vinogradov, I.S. Yasnikov, Y. Estrin, Stochastic dislocation kinetics and fractal structures in deforming metals probed by acoustic emission and surface topography measurements, Journal of Applied Physics 115(23) (2014) 233506
[54] T. Richeton, J. Weiss, F. Louchet, Dislocation avalanches: Role of temperature, grain size and strain hardening, Acta Materialia 53(16) (2005) 4463-4471.
[55] A. Vinogradov, E. Agletdinov, D. Merson, Mechanical Twinning is a Correlated Dynamic Process, Scientific Reports 9(1) (2019) 5748.
[56] E. Agletdinov, D. Drozdenko, P. Harcuba, P. Dobroň, D. Merson, A. Vinogradov, On the long-term correlations in the twinning and dislocation slip dynamics, Materials Science and Engineering: A 777 (2020) 139091.
[57] H. Hatano, Strain-Rate Dependence of Acoustic-Emission Power and Spectra in Aluminum-Alloys, Journal of Applied Physics 47(9) (1976) 3873-3876.
[58] A. Vinogradov, A. Lazarev, Continuous acoustic emission during intermittent plastic flow in α-brass, Scripta Materialia 66(10) (2012) 745-748.
[59] A. Vinogradov, A.V. Danyuk, D.L. Merson, I.S. Yasnikov, Probing elementary dislocation mechanisms of local plastic deformation by the advanced acoustic emission technique, Scripta Materialia 151 (2018) 53-56.
[60] A. Vinogradov, I.S. Yasnikov, D.L. Merson, Phenomenological approach towards modelling the acoustic emission due to plastic deformation in metals, Scripta Materialia 170 (2019) 172-176.
[61] P. Fleischmann, F. Lakestani, J.C. Baboux, D. Rouby, Spectral and Energy Analysis of Moving Ultrasonic Source - Application to Acoustic-Emission of Aluminum under Plastics Deformation, Materials Science and Engineering 29(3) (1977) 205-212.
[62] A.V. Vinogradov, V. Patlan, S. Hashimoto, Spectral analysis of acoustic emission during cyclic deformation of copper single crystals, Philosophical Magazine A 81(6) (2001) 1427-1446.
[63] C.B. Scruby, H.N.G. Wadley, J.J. Hill, Dynamic elastic displacements at the surface of an elastic half-space due to defect sources, Journal of Physics D: Applied Physics 16(6) (1983) 1069-1083.
[64] T.E.J. Edwards, Recent progress in the high-cycle fatigue behaviour of γ-TiAl alloys, Mater. Sci. Technol. 34(16) (2018) 1919-1939.
[65] F.D. Fischer, T. Schaden, F. Appel, H. Clemens, Mechanical twins, their development and growth, European Journal of Mechanics a-Solids 22(5) (2003) 709-726.
[66] W.T. Marketz, F.D. Fischer, H. Clemens, Deformation mechanisms in TiAl intermetallics - experiments and modeling, International Journal of Plasticity 19(3) (2003) 281-321.
[67] D. Peter, G.B. Viswanathan, A. Dlouhy, G. Eggeler, Analysis of local microstructure after shear creep deformation of a fine-grained duplex γ-TiAl alloy, Acta Materialia 58(19) (2010) 6431-6443.
[68] P. Sahu, Lattice imperfections in intermetallic Ti–Al alloys: an X-ray diffraction study of the microstructure by the Rietveld method, Intermetallics 14(2) (2006) 180-188.
[69] F. Louchet, B. Viguier, Modelling the flow stress anomaly in γ-TiAl II. The local pinning-unzipping model: Statistical analysis and consequences, Philosophical Magazine A 71(6) (1995) 1313-1333.
[70] D. Drozdenko, J. Čapek, B. Clausen, A. Vinogradov, K. Máthis, Influence of the solute concentration on the anelasticity in Mg-Al alloys: A multiple-approach study, Journal of Alloys and Compounds 786 (2019) 779-790.
[71] L. Rémy, Twin-slip interaction in f.c.c. crystals, Acta Metallurgica 25(6) (1977) 711-714.
[72] B.C. De Cooman, Y. Estrin, S.K. Kim, Twinning-induced plasticity (TWIP) steels, Acta Materialia 142 (2018) 283-362.
[73] M.H. Yoo, C.L. Fu, J.K. Lee, Deformation twinning in metals and ordered intermetallics-Ti and Ti-aluminides, Journal de Physique III 1 (1991) 1065.
[74] M. Yoo, Slip, twinning, and fracture in hexagonal close-packed metals, Metall and Mat Trans A 12(3) (1981) 409-418.
[75] M.H. Yoo, J.K. Lee, Deformation twinning in h.c.p. metals and alloys, Philosophical Magazine A 63(5) (1991) 987-1000.
[76] J.P. Campbell, J.J. Kruzic, S. Lillibridge, K.T.V. Rao, R.O. Ritchie, On the growth of small fatigue cracks in γ-based titanium aluminides, Scripta Materialia 37(5) (1997) 707-712.
[77] B. Simkin, A factor to predict microcrack nucleation at γ–γ grain boundaries in TiAl, Scripta Materialia 49(2) (2003) 149-154.

[78] B.A. Simkin, B.C. Ng, M.A. Crimp, T.R. Bieler, Crack opening due to deformation twin shear at grain boundaries in near-γ TiAl, Intermetallics 15(1) (2007) 55-60.
[79] T.E.J. Edwards, F. Di Gioacchino, R. Muñoz-Moreno, W.J. Clegg, The interaction of borides and longitudinal twinning in polycrystalline TiAl alloys, Acta Materialia 140 (2017) 305-316.